Numerical studies of the long-term dynamics of the 2D Navier-Stokes equations applied to ocean circulation.

Rodolfo Bermejo[1] Pedro Galán del Sastre[2]

Abstract

We present in this paper a numerical study of long-term calculations of an idealized mid-latitude ocean circulation model. The objective of this paper is twofold. First, we present an efficient semi-Lagrangia scheme for eddy resolving ocean circulation models, and second, we use the so called proper orthogonal decomposition technique to characterize the finite dimensional manifold that contains the attractor of the solution. Using a Galerkin projection on this manifold we reduce the high dimensional system obtained by the application of the finite element method, to a low-dimensional one and , thus, we can calculate the bifurcation diagram with the horizontal eddy viscosity coefficient as a control parameter.

Introduction

On the large scale, the ocean circulation system is driven by wind-stress, heat and fresh water fluxes. The wind-stress is the main driving mechanism of the surface circulation, whereas heat and fresh water fluxes are responsible of the thermohaline circulation, which is a component of the ocean circulation system with time scales ranging from decades to centuries and spatial scales extending on the whole ocean basin. Hence, the thermohaline circulation has a strong influence on the longer time scales of climate variability. On the other hand, the surface circulation driven by wind stress determines the sea surface temperature and is involved in the short time scale (up to decades) climate variability.

The mean feature of the wind stress driven circulation at mid-latitudes is the presence of a double gyre phenomenon with a strong boundary current at the lower gyre, which extends as a jet to the interior of the ocean. These gyres have a typical horizontal scale of about one thousand kilometers and are persistent and dominant. They represent the seasonal and inter-annual variability of large scale ocean surface circulation at mid-latitudes. Also, they transfer potential energy.

In order to understand the wind-stress driven circulation, the oceanographers have constructed a hierarchy of mathematical models. In this paper, we investigate numerically some properties of Quasi-Geostrophic models, which belong to the high range of this hierarchy.

The main objectives of this paper are: i) to describe an efficient semi-Lagrangian scheme to compute the numerical solution of ocean circulation models, and to compare it with the leap-frog scheme which is still used by many modelers; ii) since it has been shown the existence of global attractor for ocean models [7], we shall give a characterization of such an attractor by computing an orthonormal truncated basis of a finite dimensional manifold that contains it. To do so, we shall use the proper orthogonal decomposition technique (POD) [3], [5] and [9]. This basis together with a Galerkin projection allow to reducing the numerical Quasi-Geostrophic model to a dynamically equivalent low-dimensional non-linear ordinary differential equation system and , therefore, to computing the bifurcation diagram taking the horizontal eddy viscosity coefficient as a control parameter.

The Model

Our ocean model is a barotropic (constant density ρ_0) mid-latitude β-plane ocean domain D of constant depth H which is driven by climatological wind stresses acting upon the sea surface. For such a model, the system of primitive equations that govern the general ocean dynamics [7] can be integrated in the vertical to yield the following 2D Navier-Stokes equations

A) *Vorticity* $\omega(x,t) = \frac{\partial u_2}{\partial x_1} - \frac{\partial u_1}{\partial x_2}$

$$\begin{cases} \frac{D(\omega+f)}{Dt} = A\Delta\omega - \gamma\omega + F \ in \ D \times (0,T], \\ \omega(x,0) = \omega_0(x) \ in \ D, \\ \omega(x,t) \mid_{\partial D} = 0, \ \forall t, \end{cases} \tag{1}$$

B) *Stream function* $\psi(x,t)$

$$\begin{cases} \Delta\psi = \omega \ in \ D \times (0,T], \\ \psi \mid_{\partial D} = 0 \ \forall t. \end{cases} \tag{2}$$

We explain now the notation used in (1) and (2). f, known as the Coriolis parameter, represents the planetary vorticity of the motion due to the rotation of the Earth. The mathematical expression for f, assuming that the Earth is a perfect sphere, is $f = 2\Omega\cos\theta$, where $\Omega = 7.2526 \times 10^{-5} s^{-1}$ is the angular velocity of the Earth and θ $(0 \leq \theta \leq \pi)$ is the latitude. The β-plane approximation (see [8] for mathematical details) consists of projecting the spherical surface on its tangent plane at the point $(\psi_0, \theta_0) \in D$, and defining on such a plane a local Cartesian coordinate system (x_1, x_2) with origin at (ϕ_0, θ_0),where $x_1 = \frac{\phi - \phi_0}{a}$ denotes the west-east direction, a being the radius of the Earth, and $x_2 = \frac{\theta_0 - \theta}{a}$ denotes the south-north direction. In doing so, one substitutes the Coriolis parameter f by its linear approximation about the origin $f = f_0 + \beta x_2$, where $f_0 = 2\Omega\cos\theta_0$ and $\beta = \frac{1}{a}\frac{df}{d\theta} \mid_{\theta=\theta_0}$, and approximate the equation of motion formulated in spherical by a formulation in the local Cartesian coordinates of the tangent plane. It is considered that this is a first order approximation for studying the large scale ocean dynamics valid at mid-latitudes, say $20^o \leq \theta \leq 50^o$. The total derivative $\frac{D(\omega+f)}{Dt} = \frac{\partial\omega}{\partial t} + u_1\frac{\partial\omega}{\partial x_1} + u_2\frac{\partial\omega}{\partial x_2} + \beta\frac{\partial\psi}{\partial x_1}$, where $(u_1(x,t), u_2(x,t))$ are the components of the horizontal velocity $u(x,t)$, which are expressed in terms of the stream

function $\psi(x,t)$ as $u_1 = -\frac{\partial \psi}{\partial x_2}$ and $u_2 = \frac{\partial \psi}{\partial x_1}$. $F(x) = \frac{1}{\rho_0 H} curl_z \tau,\ \tau(x) = (\tau_1(x), \tau_2(x))$ being the climatological wind stress. A is a constant horizontal eddy viscosity coefficient and γ is a bottom friction coefficient.

To characterize the dynamics of the model it is convenient to introduce a number of external parameters which arise in the scaling of (1) and (2) as follows. Let τ_0 be typical amplitude of the climatological wind stress, then from the Sverdrup formula for large scale horizontal circulation in the interior of the ocean, one can obtain a typical horizontal velocity scale

$$U = \frac{\tau_0}{\rho_0 \beta H L^2}$$

where L is a representative horizontal length scale of ocean circulation and H is the typical depth of the ocean. Next, setting

$$(x_1, x_2) = L(x_1', x_2'),\ (u_1, u_2) = U(u_1', u_2'),\ t = UL^{-1}t',\ \tau = \tau_0 \tau',$$

where the prime symbol denotes a non dimensional variable, and performing this scaling in (1) and (2) , leads to the following non dimensional vorticity equation

$$\frac{\partial \omega}{\partial t} + J(\psi, \omega) + \frac{1}{R}\frac{\partial \psi}{\partial x_1} = \frac{1}{Re}\Delta\omega - \frac{E_B}{R}\omega + \frac{\tau_0}{R} curl_z \tau,$$

where for convenience we have dropped the symbol $'$ from the variables. $J(\psi, \omega) = \frac{\partial \psi}{\partial x_1}\frac{\partial \omega}{\partial x_2} - \frac{\partial \psi}{\partial x_2}\frac{\partial \omega}{\partial x_1}$ is the Jacobian operator, and

$$R = \frac{U}{\beta L^2}\ ,\ Re = \frac{UL}{A},\ E_B = \frac{\gamma}{\beta L}. \tag{3}$$

R is known as the *Rossby number,* E_B is called the *bottom Ekman number* and Re is the Reynolds number.

For our ocean model, a reasonable compromise is to fixing the bottom friction coefficient γ and leaving the dynamics depends on Re only, for the amplitude τ_0 is estimated from observational data.

Numerical formulation

Since the main concern of this paper is on the numerical aspects of (1) and (2), we shall assume that under proper regularity assumptions on ∂D, initial conditions for (ω, ψ) and F, (1) and (2) have a unique weak solution $(\omega, \psi) \in C(0, T : D(A) \times D(A))$, where $D(A) \subset H^2(D) \cap H_0^1(D)$, is the domain of the operator $A = -\Delta$. Furthermore, $\psi \in L^2(0, T; H_0^3(D))$. In order to find an approximate solution to (ω, ψ), we discretize the dependent variables both in time and space. For space discretization, we use the finite element method (although this is not an standard method in numerical ocean modelling studies) due to its good properties to deal with the irregular shape of the ocean coastlines and its flexibility to make local mesh refinements. As for time discretization, we present results obtained with two different schemes. The leap-frog scheme, which is still used in some of the best established numerical ocean general circulation models, and a semi-Lagrangian scheme.

Finite element approximation: generalities

Given $h_0 \in R,\ 0 < h_0 < 1$, let h be a space discretization parameter such that $0 < h < h_0$. To compute a numerical solution of (1) and (2) we generate a quasi-uniform partition D_h in $\overline{D}$ composed of elements T_j that satisfy the following conditions: *i)* Let NE be the number of elements in D_h, then $\overline{D} = \bigcup_j T_j,\ j = 1, .., NE$. *ii)* For $1 \leq j, l \leq NE,\ j \neq l$,

$$T_j \cap T_l = \begin{cases} P_i,\ a\ mesh\ point,\ or \\ \Gamma_{jl};\ a\ common\ side,\ or \\ \emptyset,\ empty\ set\ otherwiae. \end{cases}$$

iii) There is a positive constant μ such that for all $T_j,\ \frac{d_j}{h_j} > \mu$, where d_j denotes the diameter of the circle inscribed in T_j and h_j is the diameter of T_j. Next, we associate a family of finite element spaces with the partition D_h. To do so, we consider an element of reference $\widehat{T} \subset R^2$ such that for each element T_j of D_h we can define a one-to-one mapping $F_j : \widehat{T} \to T_j$ which has the property that if $\widehat{P}_m(\widehat{T})$ is the set of polynomials $\widehat{p}(\widehat{x})$ of degree $\leq m$ defined on $\widehat{T}$, then for each T_j there exists the set

$$P_m(T_j) = \{p(x), x \in T_j(x) : p(x) = \widehat{p}(F_j^{-1}(x))\}.$$

We define now the family of finite element spaces

$$\begin{gathered} V_h = \{v_h \in W^{1,\infty}(\overline{D}) : v_h \mid_{T_j} \in P_m(T_j)\ \forall T_j \in D_h\},\ and \\ V_{ho} = V_h \cap H_0^1(D) \end{gathered} \tag{4}$$

Furthermore, we also need the finite element space Z_h where the flow velocity is approximated

$$Z_h = \{u_h \in V_h \times V_h :\ u_h \cdot n \mid_{\partial D} = 0\}.$$

If M is the number of mesh point in D_h, then any element of V_h is expressed as

$$v_h = \sum_{i=1}^{M} V_i \Phi_i(x), \tag{5}$$

where $V_i = v_h(x_i),\ x_i$ being the $i - th$ mesh point, and $\{\Phi_i\}$ is the set of global nodal basis functions of V_h characterized by the property $\Phi_i(x_j) = \delta_{ij}$. Similarly, for the elements of Z_h

The finite element-leap-frog method

Let $I_N = \{0 = t_0 < t_1 <, ... < t_N = T\}$ be a partition of $[0, T]$, with a constant time step $k := t_{n+1} - t_n$ for any n. Hereafter, we shall use the notations $a^n(x)$ and a_i^n to denote $a(x, t_n)$ and $a(x_i, t_n)$ respectively. The finite element leap-frog solution to (1) and (2) consist of the pair of maps $\omega_h : I_N \to V_{h0}$ and $\psi_h : I_N \to V_{h0}$, with $m = 1$, such that for all time instant $t_{n+1} \in I_N,\ n > 0$, and $v_h \in V_{h0}$ satisfy the relations

$$\left(\alpha_1 \omega_h^{n+1}, v_h\right) + \left(kA\nabla\omega_h^{n+1}, \nabla v_h\right) = \left(\alpha_2 \omega_h^{n-1}, v_h\right) - \left(kA\nabla\omega_h^{n-1}, \nabla v_h\right) + (G^n, v_h), \tag{6}$$

and

$$\left(\nabla\psi_h^{n+1}, \nabla v_h\right) = -(\omega_h^{n+1}, v_h), \tag{7}$$

where

$$G^n = 2k\left(J(\psi_h^n, \omega_h^n) + F\right),\ \alpha_1 = 1 + k\gamma,\ \alpha_2 = 1 - k\gamma$$

and $(a, b) := \int_D abdx$ denotes the L^2- scalar product

We note that the time discretization of the viscous terms is implicit while the one of the Jacobian and forcing terms is explicitly. This makes the scheme be conditionally stable. In fact, using the arguments of [6] it can be proved that the scheme is linearly stable if there is a constant C_L independent of h and k such that

$$k\mu_1 \left|\nabla\psi_h^n\right|_{L^\infty(I_N,D)} < 1 - C_L \tag{8}$$

where μ_1 is the square root of the reciprocal of the smallest eigenvalue of $\Delta u + \mu u = 0$ in D and $u|_{\partial D} = 0$.

The finite element-semi-Lagrangian method

The semi-Lagrangian method is used to discretize (1) backwards in time along the characteristics of the operator $\frac{D}{Dt}$. The combination of finite elements and semi-Lagrangian method yields the following fractional step method.

Let $\omega_h : I_N \to V_{h0}$ and $\psi_h : I_N \to V_{h0}$, with $m = 2$, such that for all $n = 1, 2, ...$

$$\omega_h^n = \sum_{i=1}^{M} W_i^n \Phi_i(x) \text{ and } \psi_h^n = \sum_{i=1}^{M} \Psi_i^n \Phi_i(x). \tag{9}$$

The computation of (W_i^n, Ψ_i^n) is carried out through the following procedure:

A) The transport step.

Given ω_h^{n-1}, ψ_h^{n-1} and $\mathbf{u}_h^{n-1} = (u_{1h}^{n-1}, u_{2h}^{n-1}) \in Z_h$,

1) Calculate for each mesh point x_k, $k = 1, 2, ..., M$, the departure point $X_{hk}^{n-1} \equiv X_h(x_k, t_n; t_{n-1})$. To do so, we follow the scheme of [1] and set

$$X_{hk}^{n-1} = x_k - \alpha_{hk},$$

where α_{hk} is computed via the fixed point iteration

$$\alpha_{hk}^{(r+1)} = \frac{\Delta t}{2}\left[3\mathbf{u}_h^{n-1}(x_k - \frac{1}{2}\alpha_{hk}^{(r)}) - \mathbf{u}_h^{n-2}(x_k - \frac{1}{2}\alpha_{hk}^{(r)})\right].$$

The values of $\mathbf{u}_h^{n-1}(x_k - \frac{1}{2}\alpha_{hk}^{(r)})$ and $\mathbf{u}_h^{n-2}(x_k - \frac{1}{2}\alpha_{hk}^{(r)})$ are calculated by finite element interpolation.

2) Let $p(k)$ be the element of D_h where X_{hk}^{n-1} is located, and let $\left\{W_1^{n-1}, W_2^{n-2}, .., W_{NH}^{n-1}\right\}$ be the set of nodal values of ω_h^{n-1} in $p(k)$.

Calculate

$i)$ $\quad W_k^* = \omega_h^{n-1}(X_{hk}^{n-1})$ *and* $C_k = \beta(x_{2k} - X_{h2k}^{n-1})$.

$ii)$ $\quad W^+ := Max(W_1^{n-1}, ..., W_{NH}^{n-1})_{p(k)}$
$\quad\quad W^- := Min(W_1^{n-1}, ..., W_{NH}^{n-1})_{p(k)}$

$iii)$ $$\overline{W}_k^{n-1} = \begin{cases} W^+ \; if \; W_k^* > W^+, \\ W^- \; if \; W_k^* < W^-, \\ W_k^*, \; otherwise. \end{cases}$$

Finally, set

$$\begin{array}{l} \overline{\omega}_h^{n-1} = \sum_{k=1}^{M} \overline{W}_k^{n-1} \Phi_k(x) \\ C_h^{n-1} = \sum_{k=1}^{M} C_k^{n-1} \Phi_k(x), \end{array} \tag{10}$$

where $C_h^{n-1} = \frac{Df}{Dt} \mid_{t=t_{n-1}}$.

B) The diffusive step

Find $\omega_h^n \in V_{h0}$ and $\psi_h^n \in V_{h0}$ such that for all $q_h \in V_{h0}$
$i)$

$$\begin{array}{c} (\alpha_1 \omega_h^n, q_h) + \delta \left(\nabla \omega_h^n, \nabla q_h\right) = \left(\alpha_2 \overline{\omega}_h^{n-1}, q_h\right) - \\ \delta \left(\nabla \overline{\omega}_h^{n-1}, \nabla q_h\right) - \left(C_h^{n-1}, q_h\right) + \frac{\Delta t}{2} \left(F_h^{n-\frac{1}{2}}, q_h\right), \end{array} \tag{11}$$

$ii)$

$$-\left(\nabla \psi_h^n, \nabla q_h\right) = \left(\omega_h^n, q_h\right). \tag{12}$$

where $F_h^{n-\frac{1}{2}} = \frac{1}{2}(F_h^n + F_h^{*n-1})$ with $F_h^{*n-1} = \sum_{k=1}^{k=M} F_k^{*n-1} \Phi_k$ and $F_k^{*n-1} = F_h^{n-1}(X_{hk}^{n-1})$, $\alpha_1 = 1 + \frac{\gamma}{2}\Delta t$, $\alpha_2 = 1 - \frac{\gamma}{2}\Delta t$ and $\delta = \frac{\Delta t}{2} A$.

$iii)$ Find $\mathbf{u}_h^n \in Z_h$ such that for all $\mathbf{y}_h \in Z_h$

$$\left(\mathbf{u}_h^n, \mathbf{y}_h\right) = \left(rot \psi_h^n, \mathbf{y}_h\right), \tag{13}$$

where

$$rot \psi_h^n = \left(-\frac{\partial \psi_h^n}{\partial x_2}, \frac{\partial \psi_h^n}{\partial x_1}\right)$$

This scheme is unconditionall stable because taking $q_h = \omega_h^n + \overline{\omega}_h^{n-1}$ in (11) and using Theorem 3 of [4] yields

$$\| \omega_h^n \| \leq \| \omega_h^{n-1} \| + \frac{k}{2} \left(\| F^n \| + \| F^{n-1} \| \right)$$

Numerical experiments

We perform numerical experiments at different values of the horizontal eddy viscosity coefficient A, or equivalently, see (3), at different Reynolds numbers. The values of the

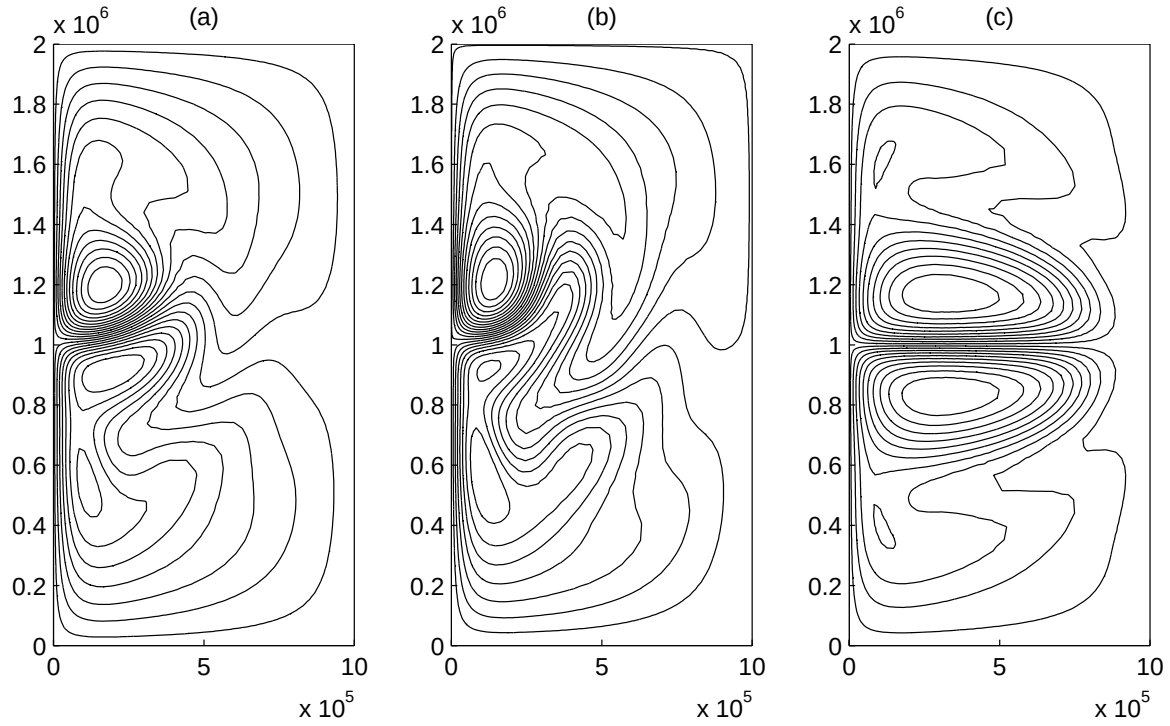

Fig. 1.

other parameters used in the experiments are

$$\begin{array}{cc} L = 10^6 m & H = 800m \\ f_0 = 5 \times 10^{-5} s^{-1} & \beta = 2 \times 10^{-11} m^{-1} s^{-1} \\ \tau_0 = 1.5 \times 10^{-4} \rho_0 & \rho_0 = 1000 kg m^{-3} \\ U = 0.03 m s^{-1} & \gamma = 10^{-7} s^{-1} \end{array}$$

We use two different meshes, one for the Leap-Frog scheme and the other one for the Semi-Lagrangian one. Both meshes have the same number of mesh points $M = 15011$, but a different number of elements $NE = 29328$ linear elements for the leap-frog scheme and $NE = 7332$ quadratic elements for the semi-Lagrangian scheme. The meshes have more elements in those regions of strong variation of the flow, such as the western boundary layer, where the size of the triangles is $5km$, and in regions where there are eddy shedding. In regions of smooth flow the size of the triangles is $40km$.

We carry out long-term ($T = 20$ *years*) numerical experiments with $A = 1000 m^2 s^{-1}$, $800 m^2 s^{-1}$, $600 m^2 s^{-1}$, $400 m^2 s^{-1}$ and $200 m^2 s^{-1}$ for both leap-frog and semi-Lagrangian schemes. A time step $k = 6$ *hours* delivers stable solutions for all the numerical runs done with the semi-Lagrangian scheme; whereas for the leap-frog scheme k has to be 1 *hour* in order to obtain stable solutions for the experiments with $A = 1000 m^2 s^{-1}$, $800 m^2 s^{-1}$, $600 m^2 s^{-1}$, and $k = 0.5 hour$ for experiments with $A = 400 m^2 s^{-1}$ and $A = 200\ m^2 s^{-1}$; although for the latter experiment the scheme become unstable after few thousand time steps.

Figures 1 (a), (b) and (c) show snapshots at $t = 10$ *years* of the stream function solution computed by the leap-frog scheme with $A = 1000 m^2 s^{-1}$, $800 m^2 s^{-1}$, and

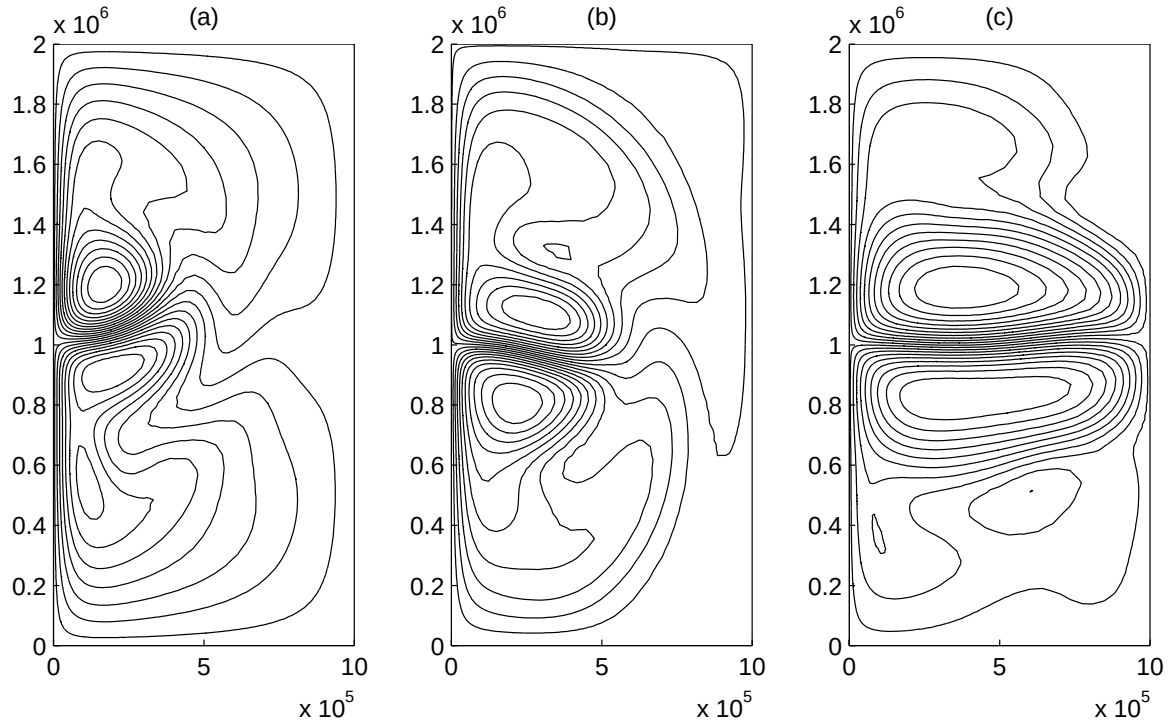

Fig. 2.

$400m^2s^{-1}$, respectively; whereas Figures 2 (a), (b) and (c) show stream function snapshots at $t = 10$ $years$ of the semi-Lagrangian solution for $A = 1000m^2s^{-1}$, $600m^2s^{-1}$ and $200m^2s^{-1}$ respectively. For $A = 1000m^2s^{-1}$ the flow converges to steady-state composed of a cyclonic gyre in the northern part of the domain and an anticyclonic one in the southern part. The two gyres are separated by a meandering jet and the northern-southern symmetry of the motion has been broken. For $A \leq 800m^2s^{-1}$ the flow does not reach the steady state.

¿From a dynamical viewpoint it is more interesting to know the time evolution and the spectrum of the kinetic energy $E(t) = \frac{1}{2}\int_D (u_1^2(t) + u_2^2(t))dx$ of the flow. These magnitudes are represented in Figures 3, and 4, in which full line pictures correspond to the semi-Lagrangian solution and broken line pictures correspond to the leap-frog solution. Thus, Figure 3 (a) represents the time history of $E(t)$ for $A = 1000m^2s^{-1}$.

Here, we notice that the flow becomes steady after about 5 $years$, and both schemes give basically the same solution. However, for $A = 800m^2s^{-1}$ and $A = 600m^2s^{-1}$, see Figures 3 $(b) - (e)$, we see that after a spin-up period of about 1 $year$ followed by a steady state which reaches a point located somewhere between the second and third year, the flow becomes periodic with principal periods of 185 days for $A = 800m^2s^{-1}$ and 220 days for $A = 600m^2s^{-1}$, respectively. Again, both schemes give similar solutions. The important point here is that the flow has undergone a Hopf bifurcation somewhere between $A = 1000m^2s^{-1}$ and $A = 800m^2s^{-1}$.

For $A = 400m^2s^{-1}$ the semi-Lagrangian solution becomes quasi-periodic with a few incommensurate frequencies, whereas the leap-frog solution remains steady after the

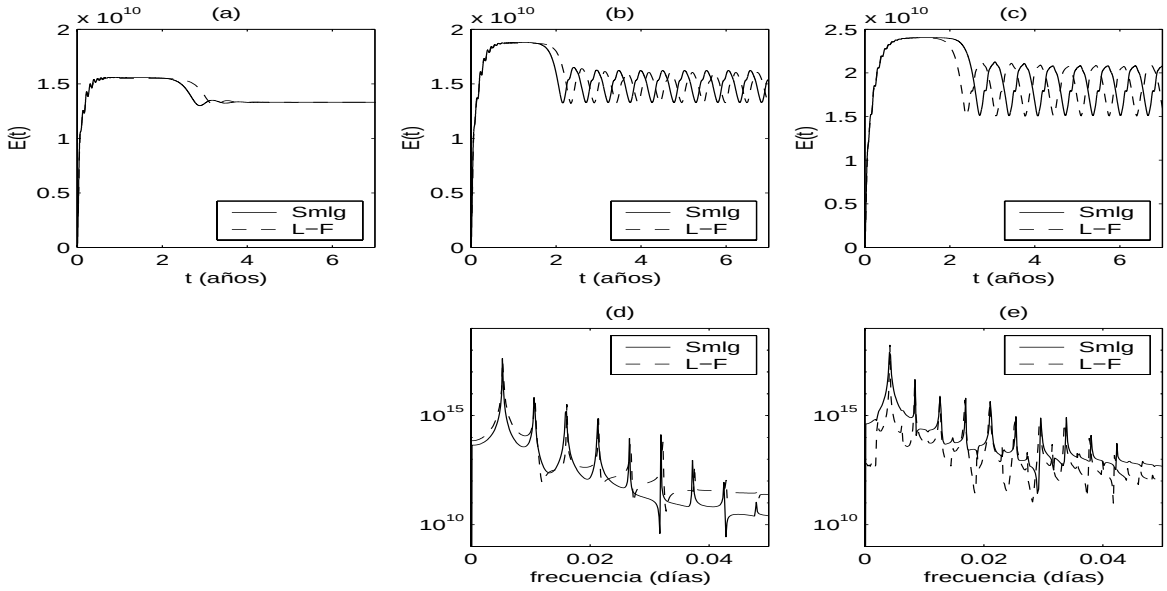

Fig. 3.

spin up period. So that, somewhere between $A = 500m^2s^{-1}$ and $A = 400m^2s^{-1}$ the periodic solutions undergo a secondary bifurcation. Our final experiment was run with $A = 200m^2s^{-1}$ and the results are shown in Figures $4(a)$ and $4(b)$. Here we see that the leap-frog solution becomes unstable after 5 *years* of integration with $k = 0.5$ *hours*, whereas the semi-Lagrangian solution, computed with $k = 6$ *hours*, exhibits a sort of a chaotic behavior as suggested by its broad band spectrum.

Summarizing, we observe that of the dynamics of the flow is composed of coherent structures both in time and space with a time history that depends on the eddy viscosity coefficient A. The flow asymptotically approaches a stable steady state for $A \geq 1000$, as A is decreased the steady state loses stability to a periodic state, which remain stable for values of A well beyond 600, for some value of A between 500 a 400 the periodic state undergoes a secondary bifurcation to a quasi-periodic flow, which then persists beyond 400. In the next section we shall draw the bifurcation diagram of the flow as a function of A.

Table 1 gives some statistics of the experiments concerning the total CPU time and CPU time per time step employed in each experiment for both methods.

All the experiments have been run on a processor *Mips R10000* to 250 MHz and with 256 Mbytes of RAM memory. We note that the CPU time spent by the semi-Lagrangian scheme per time step is about $30\% - 40\%$ lower than the one corresponding to the leap-frog scheme, this fact, together with the property of being unconditionally stable, makes the semi-Lagrangian scheme be very competitive for large scale computation as one needs to do in climate studies.

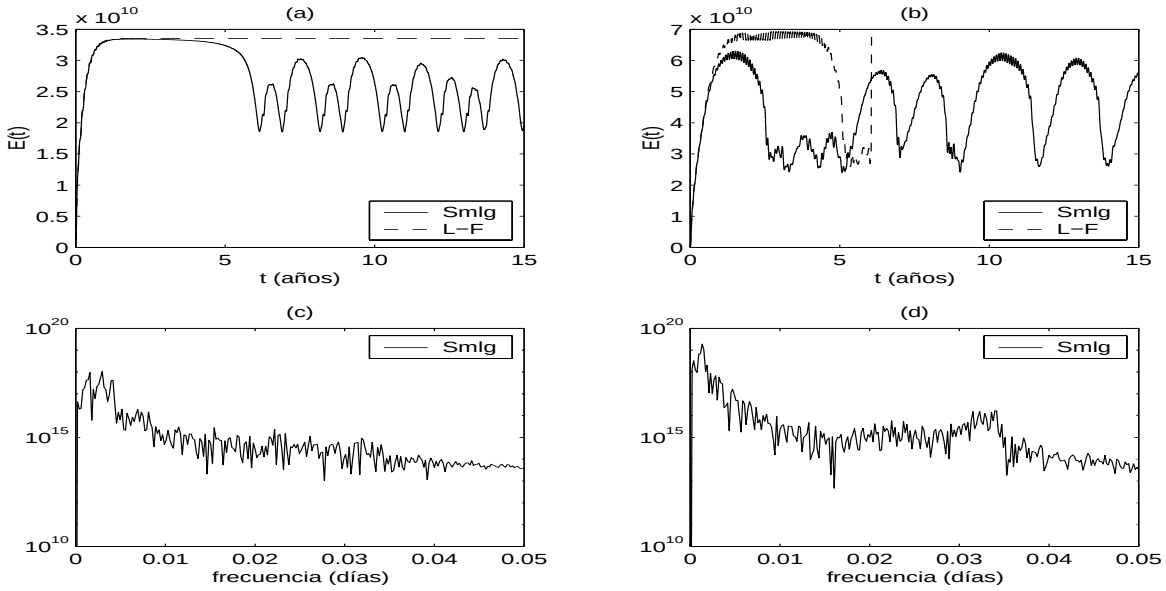

Fig. 4.

	SEMILAGRANGIANO			LEAP-FROG		
	PT	CPU	CPU/PT	PT	CPU	CPU/PT
$A_H = 1000$	29200	13587.16	0.465313	175200	199574.09	1.139121
$A_H = 800$	29200	22158.97	0.758868	175200	321110.02	1.832819
$A_H = 600$	29200	47181.17	1.615793	175200	368816.87	2.105119
$A_H = 400$	29200	20284.30	0.694667	350400	349560.64	0.997604
$A_H = 200$	29200	52026.10	1.781715	106080	119592.40	1.127379

Table 1.

Proper orthogonal decomposition (POD) technique

The focus of this section is twofold. Since there exists an attractor of system (1) and (2) see [5], first we wish to characterize the finite dimensional manifold that contains such an attractor; and second we wish to do the numerical study of the instabilities experienced by the flow as A decreases. A method to achieve this consists of reducing the system (1) and (2) to a non linear ODE system via Galerkin projection, and then to apply well known techniques to calculate the bifurcation diagram. If one does the Galerkin projection using finite elements or spectral methods, then one obtains an ODE system whose dimension is so large (of order $10^4 - 10^5$), that makes the method computationally unfeasible. There are other methods that through a post-processing procedure of the numerical solution of (1) and (2) can generate a subspace containing the approximate attractor of the system, and such that the dimension of which is computationally manageable. One of such methods is the proper orthogonal decomposition technique (POD) which generates a finite dimensional orthogonal basis

that is optimal in a sense to be defined below. An algorithmic description of this technique is as follows.

Implementation of the POD technique

Let us consider the dynamical system

$$\frac{du}{dt} = F(t, u; A),\ u(0) = u_0,\ u(t) \in H\ \forall t \in [0, T] \tag{14}$$

where H is a finite dimensional Hilbert space with scalar product $(\cdot, \cdot)$ and norm $\| \cdot \|$, and let us assume that we have a collection $\{u^i\}_{i=1}^p$ of "snapshots" of $u(t)$. In numerical computations the "snapshots" are the numerical solutions stored at predefined time steps.

Step 1 Compute

$$\overline{u} = \frac{1}{\sum_{i=1}^p \Delta\tau_{i-1}} \sum_{i=1}^p \Delta\tau_{i-1} u^i, \tag{15}$$

where $\Delta\tau_i = \tau_i - \tau_{i-1},\ \tau_i$ being the time instants at which the snapshots are stored. Then set

$$\widetilde{u}^i = u^i - \overline{u}. \tag{16}$$

Step 2 Compute the covariance matrix

$$K_{ij} = \sum_{i=1}^{p-1} \Delta\tau_i (\widetilde{u}^i, \widetilde{u}^j),\ 1 \le i, j \le p. \tag{17}$$

Notice that the matrix K is symmetric and semi-positive definite (the latter property will be proved below)

Step 3 Calculate the eigenvalues $\{\lambda_k\}$ and eigenfunctions $\{v_k\}$ of K, e.g., solve

$$Kv = \lambda v. \tag{18}$$

The base $\{v_k\}$ is ordered after decreasing eigenvalues λ_k.

Step 4 Compute the orthonormal basis $\{\varphi_k\}$, $\varphi_k \in H$, where

$$\varphi_k = \frac{\sum_{i=1}^p v_{ki} \widetilde{u}^i}{\| \sum_{i=1}^p v_{ki} \widetilde{u}^i \|} \tag{19}$$

Step 5 Cut-off criterium. If the dimension of the matrix K is too high, the procedure can become computationally unsuitable because the number of eigenfunctions to be stored may be too large. Since our interes consists of generating an orthonormal basis able to capture most of the energy of the system (we associate the energy of $u(t)$ with its L^2-norm), we shall establish a cut-off criterium to neglect those eigenfunctions with low energy content. Taking into account that the eigenvalue λ_k represents the mean

energy of the system projected on the subspace generated by the eigenfunction φ_k, a practical criterium is to store p^* eigenfunctions, $0 < p^* \leq rankK \leq p-1$, such that

$$\frac{\sum_{i=1}^{p^*} \lambda_i}{\sum_{i=1}^{p} \lambda_i} = \alpha > .99. \tag{20}$$

Hence, the dimension of the finite dimensional manifold that contains the approximate attractor of the system is p^*.

Step 6 Approximate $u(t) \in H$ as

$$u_h(t) = \overline{u} + \sum_{i=1}^{p*} a_i(t)\varphi_i. \tag{21}$$

and determine the coefficients $a_i(t),\ i = 1, 2, .., p^*$, by substituting $u_h(t)$ into (14) and performing a Galerkin projection on the $span\{\varphi_i\}_{i=1,..p^*}$. Hence, for $i = 1, 2, .., p^*$,

$$\frac{da_i}{dt} = (F(t, u_h; A), \varphi_i),\ a_i(0) = (u_{0h}, \varphi_i). \tag{22}$$

Analysis

We shall prove some important properties of the POD technique, which are the mathematical foundations of such a technique. To this end, we consider Hilbert space $H = L^2(0, T)$ with inner product and norm denoted by $(\cdot, \cdot)$ and $\| \cdot \|$, respectively, and the set $I \subset R^d,\ d \geq 1$. We introduce an average operator $\langle \cdot \rangle$ defined as

$$\begin{array}{c} \langle \cdot \rangle : L^1(I) \to R, \\ \langle u \rangle = \int_I u dx \end{array} \tag{23}$$

Hence, there exists a constant C such that

$$| \langle u \rangle | \leq C \| u \|_{L^1(I)},$$

where $\| u \|_{L^1(I)}$ denotes the L^1-norm of u. In relation with the covariance matrix K we define an operator $T : H \to H$ as follows. Given $u \in L^2(I, H)$

$$(T\phi, \varphi) = \langle (u, \phi)(u, \varphi) \rangle,\ \forall \phi, \varphi \in H. \tag{24}$$

We have the following lemma

Lemma. The operator $T : H \to H$ defined in (24) is continuous, linear, self-adjoint, semi-positive definite and compact

Proof. First, we have to prove that T is well defined, that is, $\langle (u, \phi)(u, \varphi) \rangle$ makes sense. By virtue of (23), (24) and Cauchy inequality it follows that

$$\begin{array}{c} | \langle (u, \phi)(u, \varphi) \rangle | \leq \int_I | (u, \phi)(u, \varphi) | dx \\ \leq \| \phi \| \| \varphi \| \int_I \| u \|^2 dx = \| \phi \| \| \varphi \| \| u \|^2_{L^2(I,H)} < \infty. \end{array}$$

So that, for all $\phi, \varphi \in H$ $(u,\phi)(u,\varphi)$ is in $L^1(I)$. It remains to check that $T\phi \in H$. To this end, let us assume that this true and take an orthonormal basis $\{e_k\}$ of H Then

$$T\phi = \sum_k (T\phi, e_k)e_k, \tag{25}$$

so that

$$\| T\phi \|^2 = \sum_k | (T\phi, e_k) |^2$$

and from (24) it follows that

$$\| T\phi \|^2 = \sum_k | \langle (u,\phi)(u,e_k) \rangle |^2 \leq C^2 \| \phi \|^2 \| u \|^4_{L^2(I,H)} < \infty, \tag{26}$$

where that last inequality on the right hand side has been obtained by using the same type of argument as above. Now, we go on with the proof of the lemma. It is easy to show that T is a linear, continuous, self- adjoint and semi-positive deinite operator so that we omit the prove. Next, we prove that T is a compact operator by defining a sequence of compact operators $\{T_n\}_{n\in N}, T_n : H \to H$ such that $T_n \to T$ in $\mathcal{L}(H)$ [11, X,2]. To find these operators T_n, let us consider the sequence $\{u_n\}_{n\in N} \subset L^2(I,H)$ such that $u_n \to u$ in $L^2(I,H)$ and $span\{u_n\}$ is finite. Then, we define T_n as follows: $\forall \phi, \varphi \in H$

$$(T_n\phi, \varphi) = \langle (u_n,\phi)(u_n,\varphi) \rangle.$$

So that $T_n(H) \subset \overline{span\{u_n\}}^H$, or consequently, for all n the operators T_n are of finite range. Hence, if B is the closed unite ball in H it follows that $T_n(B)$ is compact and, therefore, T_n is a compact operator. It remains to prove that $\| T_n - T \| \to 0$ as $n \to \infty$. To do so, we consider

$$\begin{aligned} ((T_n - T)\phi, \varphi) &= \langle (u_n,\phi)(u_n,\varphi) \rangle - \langle (u,\phi)(u,\varphi) \rangle \\ &= \langle (u_n,\phi)(u_n - u,\varphi) \rangle + \langle (u_n - u,\phi)(u,\varphi) \rangle. \end{aligned}$$

Then, arguing as above it is easy to see that

$$| ((T_n - T)\phi, \varphi) | \leq C \| \phi \| \| \varphi \| \{ \| u_n \|_{L^2(I,H)} + \| u \|_{L^2(I,H)} \} \| u_n - u \|_{L^2(I,H)}$$

By taking ϕ and φ such as $\| \phi \| \leq 1$ and $\varphi = (T_n - T)\phi$ yields

$$\| (T_n - T)\phi \|^2 \leq C \{ \| u_n \|_{L^2(I,H)} + \| u \|_{L^2(I,H)} \} \| u_n - u \|_{L^2(I,H)} .$$

Hence, $\| T_n - T \| \to 0$ as $n \to \infty$., and this concludes the proof. ∎

For our purposes, Lemma 1 is relevant because by virtue of Hilbert-Schmidt theorem it guaranties the existence of pairs (λ_i, ϕ_i), $i = 1, 2..., \dim H$, $\lambda_i \in R^+$, $\phi_i \in H$ being orthonormal, such that

a)

$$T\phi_i = \lambda_i \phi_i, \ 1 \leq i \leq \dim H \tag{27}$$

and all $u(t) \in H$ can be written as

$$\begin{array}{c} u(t) = \sum_i a_i(t)\phi_i, \\ a_i = (u, \phi_i),\ hence\ \ \| u \|^2 = \sum_i \mid a_i \mid^2 . \end{array} \tag{28}$$

b) Furthermore, (λ_i, ϕ_i) are the critical points of the Lagrangian $J : H \times R^+ \to R$ defined as

$$J(\varphi, \lambda) = (T\varphi, \varphi) - \lambda \| \varphi \| \tag{29}$$

It is straightforward to obtain from (27) and (28) the following relations

$$\lambda_i = (T\phi_i, \phi_i) = \langle (u, \phi_i)^2 \rangle = \langle \mid a_i \mid^2 \rangle,\ \forall i,$$

hence,

$$\sum_i \lambda_i = \sum_i \langle \mid a_i \mid^2 \rangle = \langle \| u \|^2 \rangle. \tag{30}$$

These relations are important because they are used to characterize the orthonormal basis $\{\phi_i\}$ as optimal in the sense defined in the following proposition

Proposition. Let $\{\phi_i\}$ and $\{\psi_i\}$, $1 \le i \le \dim H$, be two distinct orthonormal bases of H, ϕ_i being the i-th eigunfunction of the operator T. Let u^M and $\widetilde{u}^M$ be approximations of $u \in H$ defined as

$$\begin{array}{l} u^M(t) = \sum_i^M a_i(t)\phi_i \\ \widetilde{u}^M(t) = \sum_i^M b_i(t)\psi_i \end{array} \ ,\ M \le \dim H$$

then the basis $\{\phi_i\}$ is optimal in the sense that for all M

$$\langle \| u - u^M \| \rangle \le \langle \| u - \widetilde{u}^M \| \rangle$$

Proof. Let us represent u as

$$u = \sum_i a_i\phi_i \ and\ u = \sum_i b_i\psi_i.$$

On the other hand, since for all i $\psi_i \in H$, then we can represent it in terms of the basis $\{\phi_i\}$ as

$$\psi_k = \sum_i C_{ki}\phi_i,\ 1 \le k \le \dim H.$$

Next,

$$\langle \| u - u^M \|^2 \rangle = \langle (u - u^M, u - u^M) \rangle = \langle (\sum_{i>M} a_i\phi_i, \sum_{i>M} a_i\phi_i) \rangle = \sum_{i>M} \langle \mid a_i \mid^2 \rangle,$$

similarly

$$\langle \| u - \widetilde{u}^M \|^2 \rangle = \langle (u - \widetilde{u}^M, u - \widetilde{u}^M) \rangle = \langle (\sum_{i>M} a_i\psi_i, \sum_{i>M} b_i\psi_i) \rangle = \sum_{i>M} \langle \mid b_i \mid^2 \rangle$$

Using the representation of the basis $\{\psi_i\}$ in terms of the eigenfunctions $\{\phi_i\}$ we can set

$$b_k = \sum_{i=1}^{M} C_{ki} a_i,\ 1 \leq k \leq M,$$

and by appealing to remark 1.3 of V.I.2 of [10] we have that $\sum_{i=1}^{M} \lambda_i \geq \sum_{i=1}^{M} \langle \mid b_i \mid^2 \rangle$. Hence,

$$\sum_{i>M} \lambda_i \leq \sum_{i>M} \langle \mid b_i \mid^2 \rangle,$$

since it also holds that $\sum_i \lambda_i = \sum_i \langle \mid b_i \mid^2 \rangle,\ 1 \leq i \leq \dim H.$ ■

Next, we wish to find out the relationship between the operator T and the covariance matrix K defined in (17). Since we are working with snapshots of the numerical solution, we restrict the Hilbert space on which T is defined to a discrete finite dimensional subspace $H_{p,\Delta t} \subset H$ defined as

$$H_{p,\Delta t} = \{v = (v^1, ..., v^p \in R^p : \sum_{i=1}^{p} \Delta\tau_i \mid v^i \mid^2 < \infty\},$$

where $\tau_i \in [0, T]$ are the time instants at which the snapshots of the numerical solution are stored, $\Delta\tau_i = \tau_i - \tau_{i-1}$ and $v^i = v(\tau_i)$. The inner product in $H_{p,\Delta t}$ is defined by

$$(a, b) = \sum_{i=1}^{p} \Delta\tau_i a^i b^i;\ a, b \in H_{p,\Delta t}.$$

In relation with the average operator introduced in (23) we take $I = D$, so that for all $f \in L^1(D)$ we have that

$$\langle f \rangle = \int_D f dx.$$

Thus, given $U \equiv (u^1(x), ...u^p(x)) \in L^2(I, H_{p,\Delta t})$ and such that for $1 \leq i \leq p,\ u^i(x) \in L^2(D)$ we have that

$$\begin{aligned}(Ta, b) = \langle (U, a)(U, b) \rangle &= \textstyle\int_D (\sum_{j=1}^{p} \Delta\tau_j u^j(x) a^j)(\sum_{i=1}^{p} \Delta\tau_i u^i(x) b^i) dx \\ &= \textstyle\sum_{i=1}^{p} \sum_{j=1}^{p} \Delta\tau_i \Delta\tau_j b^i a^j (\int_D u^i(x) u^j(x) dx) \\ &= \textstyle\sum_{i=1}^{p} \Delta\tau_i b^i (\sum_{j=1}^{p} \Delta\tau_j K_{ij} a^j) = (Ka, b).\end{aligned}$$

So that, the covariance matrix K is the matrix of the operator T. We state this result in the following proposition.

Proposition. The covariance matrix K defined in (23) is the matrix associated to the operator T defined in (24).

Application of the POD technique to the barotropic ocean model

In order to compute a low dimensional dynamical system equivalent to (1) and (2), we proceed in this section to apply the POD technique as a post-processing procedure

to the finite element semi-Lagrangian solution of (1) and (2) for $A = 1000m^2s^{-1}$, $800m^2s^{-1}$, $600m^2s^{-1}$, $500m^2s^{-1}$ and $400m^2s^{-1}$. We shall start storing snapshots of the vorticity and stream-function solution after the spin-up time of the model. Looking at the energy graphs of the numerical solutions we notice that for any value of A the solution lies in the attractor after 8 years of simulation; so that, taking this value as the spin-up time of the model, we store snapshots of the vorticity and stream-function solution every 5 days for a time period of 1000 days, this makes a total of 200 snapshots for each value of A. Following the steps of Section 5.1, we compute for each A an orthonormal basis $\{\varphi_i^\omega\}_{i=1}^{p^*}$ and set

$$\begin{array}{c} \omega_h(x,t) = \overline{\omega}_h(x) + \sum_{i=1}^{p^*} a_i(t)\varphi_i^\omega \\ \psi_h(x,t) = \overline{\psi}_h(x) + \sum_{i=1}^{p^*} a_i(t)\varphi_i^\psi, \end{array} \tag{31}$$

where $\Delta_h\overline{\psi}_h(x) = \overline{\omega}_h(x)$, $\Delta_h\varphi_i^\psi = \varphi_i^\omega$, with $\Delta_h : V_{h0} \to V_{h0}$ being the discrete Laplacian operator. The unknowns $\{a_i(t)\}$ are determined by substituting (31) into (1) and (2) and performing a Galerkin projection on the subspace generated by the orthonormal basis $\{\varphi_i^\omega\}_{i=1}^{p^*}$. By doing so we obtain

$$\frac{da_i}{dt} = \sum_{j,k=1}^{p^+} a_j(t)a_k(t)D_{jki} + \sum_{j=1}^{p^+} a_jQ_{ji} + R_i,\ 1 \le i \le p^*. \tag{32}$$

where

$$\begin{array}{c} D_{jki} = -(J(\varphi_j^\psi, \varphi_k^\omega), \varphi_i^\omega) \\ Q_{ji} = A_{ji} + B_{ji} - \beta C_{ji} + AE_{ji} - \gamma\delta_{ji} \\ R_i = \left(-J(\overline{\psi}_h, \overline{\omega}_h) - \beta\frac{\partial\overline{\psi}_h}{\partial x} + A\Delta_h\overline{\omega}_h - \gamma\overline{\omega}_h + F, \varphi_i^\omega\right), \end{array}$$

with

$$\begin{array}{c} A_{ji} = -(J(\overline{\psi}_h, \varphi_j^\omega), \varphi_i^\omega) \\ B_{ji} = -(J(\varphi_j^\omega, \overline{\omega}_h), \varphi_i^\omega) \\ C_{ji} = \left(\frac{\partial\varphi_j^\psi}{\partial x}, \varphi_i^\omega\right) \\ E_{ji} = (\Delta_h\varphi_j^\omega, \varphi_i^\omega) \\ I_{ji} = (\varphi_j^\omega, \varphi_i^\omega) = \delta_{ji}. \end{array}$$

To determine $a_i(t)$ we solve (32) by a numerical method. In the results we show below we have employed the Runge-Kutta Fehlberg4(5) method.

Numerical examples

We show here POD results obtained by solving (32) with different values of A. As we mentioned above, in each experiment we have collected 200 snapshots of the vorticity solution at intervals of 5 days after the spin-up time (about 8 years) of the experiment. Table 2 gives information of the fraction of the total energy represented by truncating the set of POD eigenfunctions for $A = 800m^2s^{-1}$

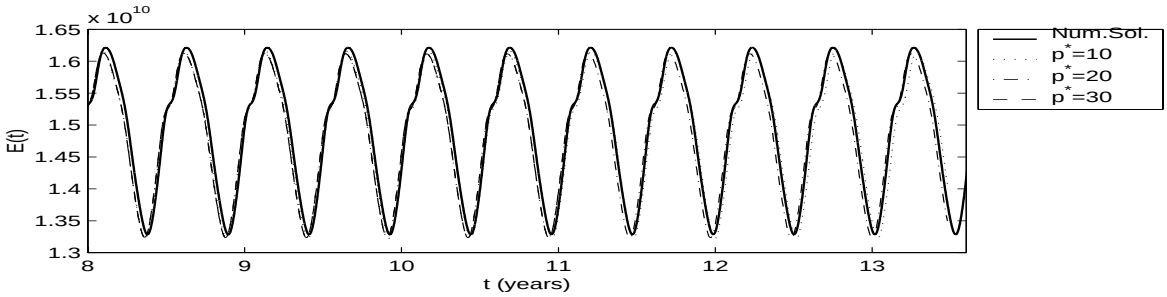

Fig. 5.

$A = 800m^2s^{-1}$	*Total Kinet. Energy*
$p^* = 10$	99.96445538%
$p^* = 20$	99.99992594%
$p^* = 30$	99.99999986%

Table 2.

Thus, we see that the first 10 eigenfunctions (or modes) are able to represent the dynamics up to a level of 99.96445538% of the total kinetic energy. Figure 5 shows the energy graphs of the direct numerical solution and of the POD solution for 10, 20 and 30 modes.

We notice the good agreement between the direct numerical solution and the POD one even with just only 10 modes. For $A = 600$ things are a little bit different. The dimension of the attractor is larger, so that we expect to need more modes representing the dynamics. This is confirmed by the results shown in Table 3.

$A = 600m^2s^{-1}$	*Total Kinet. Energy*
$p^* = 10$	99.24121041%
$p^* = 30$	99.99898548%
$p^* = 50$	99.99998724%
$p^* = 60$	99.99999696%

Table 3.

Figure 6 shows the energy graphs of the direct numerical solution and of POD solutions for 10, 30 and 60 modes. We see that 10 modes do not give a good representation; however, the POD solution with 60 modes is very good, although 30 modes are also able to give an acceptable solution.

Table 4 and Figure 7 give the POD results for $A = 400m^2s^{-1}$

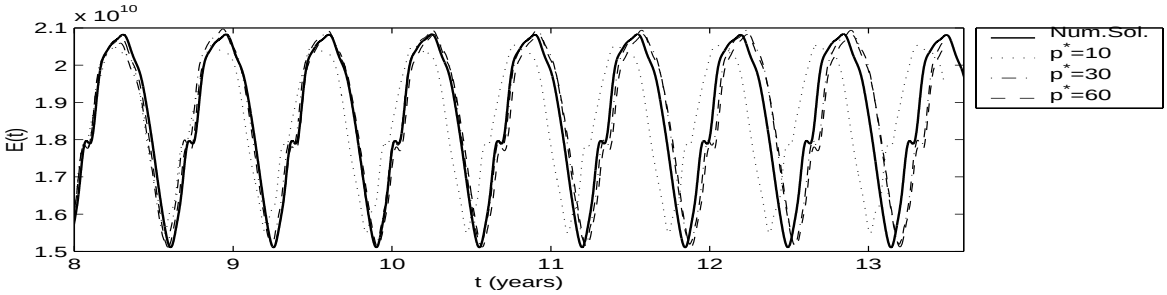

Fig. 6.

$A = 400m^2s^{-1}$	$Total\ Kinet.\ Energy$
$p^* = 20$	98.86859836%
$p^* = 40$	99.84382625%
$p^* = 80$	99.99481342%
$p^* = 90$	99.99788447%

Table 4.

In this table we notice that the dynamics of the quasi-periodic solution requires a number of POD modes much higher than that of the periodic dynamics just only to approximate 99.998% of the total kinetic energy. In Figure 7 we see that in order to get an acceptable POD solution we need 80 modes. We show in Figure 8 the bifurcation diagram of the model which is obtained by using AUTO97 to the integrate (32) with the horizontal eddy viscosity coefficient A being now the control parameter. The POD orthonormal basis used for this purpose has been generated by combining 14 POD eigunfunctions of the basis for $A = 800m^2s^{-1}$ with 30 eigunfunctions of the basis for $A = 500m^2s^{-1}$ plus 1 POD eigunfunction of the basis for $A = 1000m^2s^{-1}$. In the diagram, drawn (dash) branches denote stable (unstable) states, whereas bifurcation points are indicated by square marks for Hopf bifurcation points, and triangular marks for critical points. The steady solution becomes unstable and undergoes a Hopf bifurcation at $A = 881.71$. The periodic solution is not structurally stable and experiences a new Hopf bifurcation at $A = 410.23$. to become a quasi-periodic solution, which neither is structurally stable. Thus, as A decreases the quasi-periodic solution passes through two critical points at $A = 314, 77$, in which the solution reverses, and at $A = 297.77$.

References

[1] A. Alievi, R. Bermejo, "A Generalized Particle Search-Locate Algorithm for Arbitrary Grids ", *Journal of Comput. Physics.*, **132**, (1997).

[2] A. Alievi, R. Bermejo, "Finite Element Modified Method of Characteristics for the Navier-Stokes Equations," *Int. J. Numer. Methods in Fluids*, **32**, (2000), 439-464.

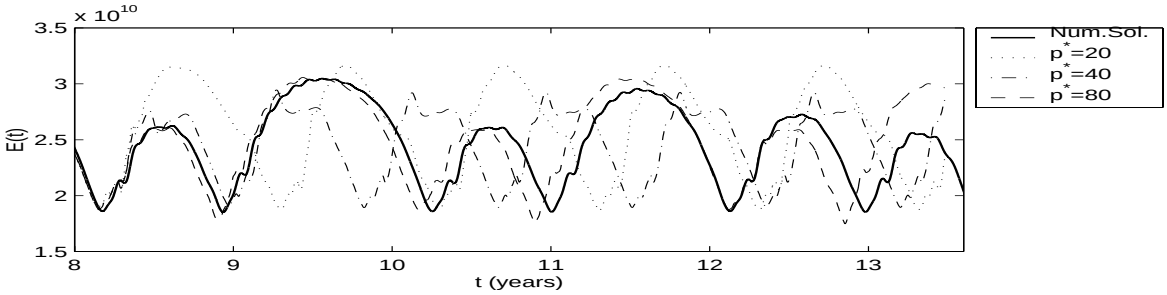

Fig. 7.

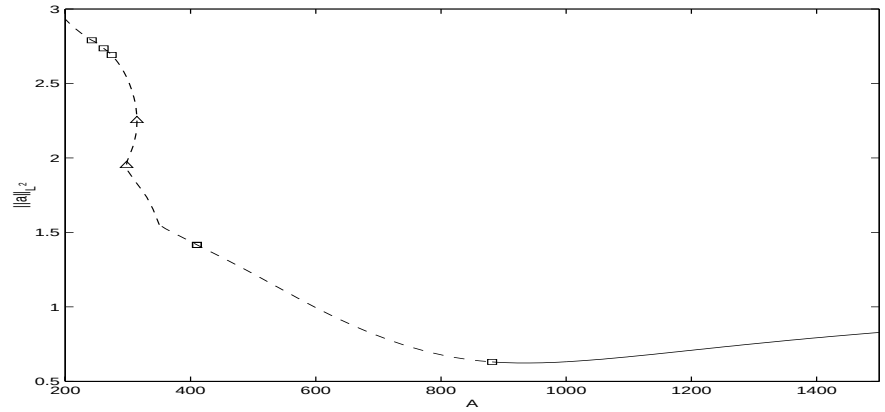

Fig. 8.

[3] R. Bermejo, " Analysis of a Class of Quasi-Monotone and Conservative Semi-Lagrangian Advection Schemes, *Numer. Math.*, **87**,4, (2001), 597-623.

[4] G. Berkooz, P. Holmes, J. L. Lumley, The Proper Orthogonal Decomposition in the Analysis of Turbulent Flows, *Annual Review of Fluid Mechanics,* **25**, (1993), 539-575.

[5] P. Holmes, J. L. Lumley, G. Berkooz, *Turbulence, Coherent Structures, Dynamical Systems and Symmetry.* Cambridge University Press (1996).

[6] H-O Kreiss, *Numerical Methods for Solving Time-Dependent Problems for Partial differential Equations.* Le Presses de L'Universit de Montreal (1978).

[7] J.L. Lions, R. Temam, S Wang, On the Equations of Large Scale Ocean,*Nonlinearity,* **5**, (1992), 1007-1053.

[8] J. Pedlosky, *Geophysical Fluid Dynamics.* Springer Verlag (1987).

[9] L. Sirovich,Turbulence and the Dynamics of Coherent Structures, Part I, *Quarterly of Applied Math.* **XLV**, 3, (1987), 561-571.

[10] R. Temam, *Infinite-Dimensional Systems in Mechanics and Physics*, Springer Verlag, (1988).

[11] K. Yosida *Functional Analysis*, Springer Verlag, (1980).

1 Departamento de Matemática Aplicada. Universidad Complutense de Madrid. Ciudad Universitaria, 28040 Madrid. rbermejo@amb-to.uclm.es

2 Departamento de Matemática Aplicada. Universidad Complutense de Madrid. Ciudad Universitaria, 28040 Madrid. pedro_galan@mat.ucm.es